

1 **A GCM Comparison of Pleistocene Super-Interglacial Periods in**
2 **Relation to Lake El'gygytgyn, NE Arctic Russia**

3
4 Anthony J. Coletti¹, Robert M. DeConto¹, Julie Brigham-Grette¹, Martin Melles²

5
6 [1] Department of Geosciences, University of Massachusetts, Amherst, MA, 01003, USA

7 [2] Institute of Geology and Mineralogy, University of Cologne, Zuelpicher Strasse 49a, D-
8 50674 Cologne, Germany

9
10
11 **Abstract**

12
13 **Until now, the lack of time-continuous, terrestrial paleoenvironmental data**
14 **from the Pleistocene Arctic has made model simulations of past interglacials**
15 **difficult to assess. Here, we compare climate simulations of four warm interglacials**
16 **at Marine Isotope Stage (MIS) 1 (9ka), 5e (127 ka), 11c (409 ka), and 31 (1072 ka)**
17 **with new proxy climate data recovered from Lake El'gygytgyn, NE Russia. Climate**
18 **reconstructions of the Mean Temperature of the Warmest Month (MTWM) indicate**
19 **conditions up to 0.4, 2.1, 0.5 and 3.1 °C warmer than today during MIS-1, 5e, 11c,**
20 **and 31, respectively. While the climate model captures much of the observed**
21 **warming during each interglacial, largely in response to boreal summer (JJA)**
22 **orbital forcing, the extraordinary warmth of MIS-11c relative to the other**
23 **interglacials in the Lake El'gygytgyn temperature proxy reconstructions remains**
24 **difficult to explain. To deconvolve the contribution of multiple influences on**
25 **interglacial warming at Lake El'gygytgyn, we isolated the influence of vegetation,**
26 **sea ice, and circum-Arctic land ice feedbacks on the modeled climate of the**
27 **Beringian interior. Simulations accounting for climate-vegetation-land surface**
28 **feedbacks during all four interglacials show expanding boreal forest cover with**
29 **increasing summer insolation intensity. A deglaciated Greenland is shown to have a**
30 **minimal effect on Northeast Asian temperature during the warmth of stage 11c and**
31 **31 (Melles et al., 2012). A prescribed enhancement of oceanic heat transport into the**

32 **Arctic Ocean does have some effect on Lake El'gygytyn regional climate, but the**
33 **exceptional warmth of MIS-11c remains enigmatic relative to the modest orbital and**
34 **greenhouse gas forcing during that interglacial.**

35

36

37 **1. Introduction**

38

39 Knowledge of Pleistocene climate history has increased dramatically over the past
40 three decades, however existing records remain strongly biased toward an oceanic
41 viewpoint, due to the lack of long terrestrial archives. In the context of future warming, it
42 is clearly important to understand the effects of warming on the terrestrial Arctic, the
43 strength of polar amplification, and systemic teleconnections to and from other latitudes.
44 Past warm periods known as Interglacials, over the past 2.8 million years, provide a
45 means of studying climates warmer than today.

46 In 2009, a multinational team drilled a sediment core from a 25 km wide impact
47 crater lake named Lake El'gygytyn (alternatively, Lake "E"), in northeast Siberia
48 (Brigham-Grette et al., 2013; Melles et al., 2012). The core contains the longest Arctic
49 terrestrial record ever recovered, extending back ~3.5 million years, and provides
50 evidence for periods of exceptional warmth during Pleistocene interglacials as defined by
51 marine benthic $\delta^{18}\text{O}$ records (Lisiecki and Raymo, 2005) (Fig. 1A&B). It has been shown
52 that Marine Isotope Stage(s) 1, 5e, 11c and 31 were among the warmest interglacials in
53 the Pleistocene Arctic (Melles et al., 2012).

54 To explore the sensitivity of northwestern Beringia to interglacial forcing and the
55 mechanisms responsible for the observed climate changes, we use a Global Climate
56 Model coupled to an interactive vegetation model to simulate the terrestrial Arctic's
57 response to the greenhouse gas and astronomical forcing associated with specific
58 interglacial (e.g., Yin and Berger, 2011). A range of sensitivity tests were performed and
59 changes in boundary conditions are imposed to test the response of the region to changes
60 in circum-Arctic ice sheets and possible changes of ocean heat transport into the Arctic
61 Ocean. In this text, we will outline changes in radiative forcing attributed to orbital
62 changes while also outlining changes in temperature, precipitation and vegetation in

63 detail, assumed to also be related to these changes. The results are then compared to the
64 Lake E multi-proxy reconstructions.

65

66 **2. Model and experimental design**

67

68 All global climate simulations discussed herein were performed using the current
69 version of the Global ENvironmental and Ecological Simulation of Interactive Systems
70 (GENESIS) Global Climate Model (GCM) version 3.0 (Alder et al., 2011; Thompson and
71 Pollard, 1997). GENESIS is an atmosphere, land-surface, ocean, snow, sea ice, ice sheet
72 and vegetation coupled model. As used here, spectral resolution of the atmosphere GCM
73 is a T31 resolution (approximately 3.75° resolution) with 18 vertical levels (Thompson
74 and Pollard, 1997). The AGCM is coupled to 2°x2° soil, snow, vegetation, ocean, and sea
75 ice model components. The GCM is interactively coupled to the BIOME4 (Kaplan, 2003)
76 vegetation model that predicts equilibrium vegetation distribution, structure and
77 biogeochemistry using monthly mean climatologies of precipitation, temperature and
78 clouds simulated by the GCM. Vegetation distributions take the form of 27 plant biomes
79 including 12 plant functional types (PFTs) that represent broad, physiologically distinct
80 classes (Kaplan, 2003). GENESIS includes options for coupling to an Ocean General
81 Circulation Model (Alder et al., 2011) or a non-dynamical, slab ocean model that
82 incorporates heat transfer, calculations of sea-surface temperatures (SST) and feedbacks
83 operating between ocean surface and sea ice. The slab mixed layer ocean model is used
84 here to allow multiple simulations to be performed with and without imposed
85 perturbations of surface ocean conditions. This version of the GCM has a sensitivity of
86 2.9 °C, without GHG, vegetation or ice sheet feedbacks. Greenhouse gases and orbital
87 parameters for each interglacial simulation were prescribed according to ice core records
88 (Louergue et al., 2008; Lüthi et al., 2008; Schilt et al., 2010) and standard astronomical
89 solutions (Berger, 1978).

90 The strategy adopted here was to target Marine Isotope Stage (MIS) 1 (11 ka), 5e
91 (127 ka), 11c (409 ka) and 31 (1072 ka), corresponding to the timing of peak summer
92 (July) warmth observed at Lake E and identified as “super-interglacials” by Melles et al.,
93 (2012). Equilibrium simulations were performed at the time of peak boreal summer

94 insolation at 67.5°N (Berger, 1978) assuming the real climate system equilibrated within
95 a half-precession cycle. Model temperature and precipitation values were calculated from
96 20-year averages taken from the 60 to 80-year equilibrated simulations. Preliminary
97 analysis of pollen assemblages in the Lake E core is assumed to provide a record of peak
98 summer temperatures, hence our data-model comparisons focus on warmest monthly
99 mean climate (July). A simulation of preindustrial climate (280 ppmv $p\text{CO}_2$) was run as a
100 control experiment to evaluate the model's representation of Beringian climate and to
101 provide a baseline for comparing super-interglacial simulations. A modern Greenland Ice
102 Sheet (GIS) is prescribed unless otherwise noted. In simulations without a GIS, the ice
103 sheet is replaced with ice-free, isostatically equilibrated land surface elevations.

104

105 **2.1 MIS 1, 9 ka**

106

107 MIS-1 represents the last ~11,000 years and its onset roughly coincides with the
108 end of the Younger-Dryas (~11,500 ka). Peak boreal summer insolation occurs ~9 ka,
109 when summer insolation was ~510 Wm^{-2} at 65 °N, relative to 446 Wm^{-2} today. Proxy
110 indicators suggest conditions were warmer than present (+1.6 °C over western Arctic and
111 +2 to 4°C in circum-Arctic) with lush birch and alder shrubs (Melles et al., 2012)
112 dominating the vegetation around the lake. This period, known as the Holocene Climate
113 Optimum (HCO), was spatially variable, with most warming in the high latitudes, and
114 minimal warming in the mid-latitudes and tropics (Kitoh and Murakami, 2002).

115

116 **2.2 MIS-5e, 127 ka**

117 MIS-5e, also known as the Last Interglaciation (LIG), is one of the warmest
118 interglacials of the Pleistocene and lasted roughly ~14 ka (130 to 116 ka). High obliquity,
119 eccentricity and the timing of perihelion (precession) combined to produce high intensity
120 boreal summer insolation at around 127 ka. Greenland ice core records (Dahl-Jensen and
121 NEEM community members, 2013) suggest summer warming up to 8 ± 4 °C over
122 northeast Greenland, but only a modest reduction in the size of the Greenland Ice Sheet
123 (GIS). Studies involving Sr – Nd – Pb isotope ratios of silt-sized sediment discharged
124 from southern Greenland suggest that no single southern Greenland geologic terrain was

125 completely deglaciated during the LIG, however, some southern GIS retreat was evident
126 (Colville et al., 2011). A previous model study of MIS-5e by (Yin and Berger, 2011)
127 involved running a model of intermediate complexity to test relative contributions of
128 Greenhouse Gas (GHG) and insolation forcing on LIG warmth. They found that GHGs
129 play a dominant role on the variations of the annual mean temperature of both the globe
130 and the southern high latitudes, whereas, insolation plays a dominant role on
131 precipitation, northern high latitude temperatures, and sea ice extent (Yin and Berger,
132 2011). Similarly, model simulations have shown that insolation anomalies during MIS-5e
133 likely caused significant summer (JJA) warming throughout the Arctic (Bakker et al.,
134 2013; Lunt et al., 2013; Otto-Bliesner et al., 2006).

135 The LIG simulation shown here is used to compare paleoenvironmental
136 conditions in western Beringia, including, temperature, vegetation and precipitation, to
137 Lake E pollen proxy analysis. Orbital parameters and greenhouse gas concentrations are
138 set at their 127 ka values to represent peak boreal warmth during MIS-5e.

139

140 **2.3 MIS-11c, 409 ka**

141

142 MIS-11c is another exceptionally warm interglacial (Howard, 1997) that lasted
143 from 428 to 383 ka (~45 ka). Sediment records from the Arctic containing information on
144 MIS-11 are generally lacking (Miller et al., 2010b). Unlike the other interglacials, MIS-
145 11c was remarkably long, with two boreal insolation maxima at ~409 ka and 423 ka,
146 creating extensive warmth throughout the Arctic (Melles et al., 2012). Unlike MIS-5e,
147 there is evidence that the GIS may have been reduced in size (Raymo and Mitrovica,
148 2012; Willerslev et al., 2007), with lush boreal forest covering most of southern
149 Greenland (de Vernal and Hillaire-Marcel, 2008). Particularly warm conditions are also
150 suggested by pollen records analyzed from Lake Biwa (Tarasov et al., 2011) located in
151 Shiga Prefecture, Japan. Likewise, a study from Lake Baikal also indicates warmer than
152 modern temperatures with a “conifer optimum” suggesting warmer conditions and less
153 aridity, perhaps influenced by higher sea levels and reduced continentality (Prokopenko
154 et al., 2010).

155 Three different simulations (Table 1, 2) were run to test the sensitivity of the lake
156 region to MIS-11c forcing. The first simulation uses default boundary conditions,
157 including a modern GIS (MIS11GIS). The second simulation tests the sensitivity of the
158 Lake E region to an ice-free Greenland (MIS11NG). In this simulation, the entire GIS
159 was removed and replaced with bare soil, and the topography of Greenland was corrected
160 for glacial isostatic adjustment. The final sensitivity experiment includes an increase in
161 sub-sea ice surface heat flux from 2 Wm^{-2} in our preindustrial control, to 10 Wm^{-2}
162 (additional $+8 \text{ Wm}^{-2}$) to test the Beringian sensitivity to a mostly ice-free Arctic Ocean.
163 The increased heat flux assumes an extreme ~ 3 Sverdrup (Sv) increase in Bering Strait
164 through flow and a $4 \text{ }^\circ\text{C}$ temperature contrast between North Pacific and North Polar
165 surface water (Melles et al., 2012, supplemental). The additional heat flux convergence is
166 used to crudely mimic the influence of a wider and deeper Bering Strait during times of
167 higher sea level. Using the predictive BIOME4 interactive vegetation model, direct
168 comparisons of observed and modeled Arctic vegetation within the Lake E region can be
169 made. Furthermore, simulations using prescribed distributions of biome flora can be used
170 to quantify the local effect of changing vegetation cover around the region.

171

172 **2.4 MIS-31, 1072 ka**

173

174 MIS-31 (~ 1062 - 1082 ka) (Lisiecki and Raymo, 2005) has only been identified in
175 a few Arctic records prior to Lake E. The Interglacial represents one of the last 41-ka
176 glacial cycles and is best known for extreme warmth in circum-Antarctica ocean waters
177 induced by a deterioration of the Polar Front (Scherer et al., 2008) and the collapse of the
178 marine based West Antarctic Ice Sheet (WAIS) (DeConto et al., 2012; Pollard &
179 DeConto, 2009), by intrusion of warm surface waters onto Antarctic continental shelves.
180 On Ellesmere Island, Fosheim Dome includes terrestrial deposits that date to ~ 1.1 Ma,
181 which contains fossil beetle assemblages dated within MIS-31, suggesting temperatures
182 of 8 to $14 \text{ }^\circ\text{C}$ above modern values (Elias and Matthews Jr., 2002). It is speculated, like
183 MIS-11c, that the Arctic may have been too warm to support a GIS which may have been
184 substantially reduced in size, or possibly nonexistent (Melles et al., 2012; Raymo and

185 Mitrovica, 2012). Therefore, simulations of MIS-31 are run both with and without a GIS
186 (Table 1, 2).

187

188 **3. Results**

189 **3.1 Control Simulation**

190 **3.1.1 Preindustrial**

191

192 Simulations of preindustrial 2-m mean annual temperature (MAAT) and MTWM
193 (July) at Lake E are -12 and 10.3 °C respectively. Preindustrial summer temperatures (8
194 °C) are -2.2 °C lower than modern. GHG radiative forcing from a combination of CO₂,
195 CH₄, and N₂O atmospheric mixing ratios implies a 1.8 Wm⁻² reduction relative to
196 modern, accounting for most of the cooling in the preindustrial simulation. Generally,
197 mean annual precipitation (PANN) values in the cooler, preindustrial simulation are
198 slightly lower than modern precipitation. At Lake E, preindustrial annual precipitation
199 was 438 mm year⁻¹. Winter (DJF) precipitation in the preindustrial simulation was ~24
200 mm month⁻¹, while mean summer (JJA) precipitation was 43 mm month⁻¹.

201 Simulated preindustrial vegetation distributions are assumed to be in equilibrium
202 (Fig. 2A). In the preindustrial simulation, shrub tundra dominates the Lake E region, with
203 evergreen taiga and deciduous forests maintained in interior Siberia and Yukon.
204 Simulated Siberian biome distributions are similar to modern day vegetation described by
205 Kolosova (1980) and Viereck & Little Jr (1975). Shrub tundra in the preindustrial
206 simulation can be attributed to cool and dry Arctic conditions in the preindustrial run.

207

208 **3.2 Paleoclimate simulations**

209 **3.2.1 MIS-1 (9 ka); Holocene Thermal Maximum**

210

211 July temperatures at Lake E in the MIS-1 simulation (12.4 °C) are ~2.1 °C
212 warmer than preindustrial (10.3 °C) and summer (JJA) temperatures are 1.6 °C warmer
213 (Fig. 3A). Overall, the Siberian interior warms > 5 °C in July, relative to preindustrial.
214 Simulated MTWM exceed > 2 °C around Lake E.

215 Simulated MIS-1 PANN values at the lake ($\sim 438 \text{ mm year}^{-1}$) are close to
216 preindustrial values, although somewhat drier conditions dominate further inland,
217 possibly a result attributed to increased proximity away from a moisture source.
218 Simulated vegetation around Lake E is close to the transition between dominant shrub
219 tundra to the east and deciduous forest to the west (Fig. 2B).

220

221 **3.2.2 MIS-5e (127 ka)**

222

223 Overall warming of the Beringian interior in the MIS-5e simulation is $> 2 \text{ }^\circ\text{C}$
224 relative to preindustrial temperatures (Fig. 3B). Most of this warming can be attributed to
225 the direct effects of the MIS-5e orbit (Groll et al., 2005; Langebroek and Nisancioglu,
226 2014), which produces an Arctic summer insolation anomaly of $>50 \text{ Wm}^{-2}$ at the top of
227 the atmosphere, relative to a preindustrial (modern) orbit (Fig. 4B). According to ice core
228 records, carbon dioxide (CO_2) concentrations during this period were about 287 ppmv
229 (Hönisch et al., 2009), contributing 0.132 Wm^{-2} more surface radiative forcing than
230 preindustrial, but the combination of CO_2 , CH_4 , and N_2O attributes 0.0035 Wm^{-2} less
231 forcing relative to preindustrial GHG mixing ratios.

232 Comparing MIS-5e with respect to the preindustrial control simulation at Lake E
233 shows differences in summer (JJA) and MTWM temperatures of $+2.5$ and $+4.2 \text{ }^\circ\text{C}$,
234 respectively (Fig. 3B). Summer warming over the GIS is $+5 \text{ }^\circ\text{C}$ relative to preindustrial,
235 which is comparable to the LIG warming reported in a recent Greenland ice core study
236 (Dahl-Jensen and NEEM community members, 2013). Mean annual precipitation at Lake
237 E ($\sim 401 \text{ mm year}^{-1}$), is 37 mm year^{-1} less than preindustrial levels, and the difference is
238 statistically significant at the 95% confidence level with a p-value of 0.029. Overall,
239 similar precipitation patterns are seen at Lake E, relative to MIS-5e and the preindustrial
240 control scenario, which reflects both the overall wet bias in the GCM and the similar
241 continental/ice sheet boundary conditions, in both simulations.

242 A less moist, but warm high latitude environment produces deciduous taiga and
243 evergreen taiga biome distributions around Lake E (Fig. 2C), with evergreen taiga being
244 the most dominant in eastern Beringia and deciduous taiga being more dominant around
245 the Lake E region and most of western Beringia.

246

247 **3.2.3 MIS-11c (409 ka)**

248

249 Due to an eccentricity minimum, MIS-11c is a longer interglacial than the other
250 interglacials in this study (Howard, 1997). We assume an ice-free Greenland in our MIS-
251 11c simulations, with the ice sheet removed and replaced with isostatically equilibrated
252 (ice-free) land elevations. Additional experiments including an imposed increase in sub-
253 sea ice heat flux in the Arctic Ocean basin will also be discussed.

254 Model simulations show summer insolation anomalies (relative to preindustrial)
255 during MIS-11c ranging from $+45 - 55 \text{ Wm}^{-2}$ (Fig. 4C) allowing temperatures over the
256 Lake E region during July (month of maximum insolation) to increase $2.2 \text{ }^{\circ}\text{C}$ relative to
257 preindustrial. Overall, mean annual summer temperatures (JJA) over the circum-Arctic
258 and Lake E are 2 to $4 \text{ }^{\circ}\text{C}$ warmer than preindustrial temperatures, with the Siberian
259 interior warming the most (Table 2).

260 In MIS-11c simulations performed with (MIS11GIS) and without a GIS
261 (MIS11NG), the effect on temperature at the Lake E is shown to be small ($\sim 0.3 \text{ }^{\circ}\text{C}$).
262 Geopotential height anomalies at 500hPa ($+4 - 10$ meters) indicate upper-level warming
263 east of Lake E, and cooling west of Lake E, but the net effect of ice sheet loss on surface
264 air temperatures is mostly limited to Greenland itself and the proximal ocean, with little
265 effect at the distance of Lake E, as shown in other modeling studies (Koenig et al., 2012;
266 Otto-Bliesner et al., 2006).

267 The warm MIS-11c climate and possible reductions of Greenland and West
268 Antarctic ice sheet sheets are thought to have contributed to sea levels as much as >11
269 meters (Raymo and Mitrovica, 2012) higher than today. Arctic sea ice was also possibly
270 reduced (Cronin et al., 2013; Polyak et al., 2010). In order to test the influence of high
271 sea levels and a mostly ice-free Arctic Ocean on Lake E climate, heat flux convergence
272 under sea ice was increased from 2 Wm^{-2} to 10 Wm^{-2} in the slab ocean/dynamic sea ice
273 model. The resulting reductions in sea ice extent and warmer ($\sim 0.2 - 1.0 \text{ }^{\circ}\text{C}$) (Fig. 5A)
274 Arctic SST's produced negligible warming around Lake E ($< 0.7 \text{ }^{\circ}\text{C}$), suggesting the
275 Lake E region was relatively insensitive to Arctic Ocean conditions.

276 Precipitation amounts at Lake E during MIS11GIS are greater than preindustrial
277 values (438 mm year⁻¹). Also, MIS11NG exhibits the same precipitation amounts as our
278 preindustrial control run (~438 mm year⁻¹) (Table 2). Simulated precipitation conditions
279 in the Arctic Ocean basin are fairly dry, ~200 mm year⁻¹, comparable to reanalysis data
280 sets (Serreze and Hurst, 2000). On the contrary, simulations of MIS11NG show reduced
281 precipitation amounts by -37 mm year⁻¹ relative to MIS11GIS. Runs with increased sub-
282 ice oceanic heat flux reduced the drying seen in the MIS11NG simulation and produced
283 values greater than the preindustrial control (~475 mm year⁻¹).

284 A warmer and wetter MIS-11c places Lake E on the border of evergreen taiga and
285 shrub tundra biomes (Fig. 2D). Vegetation limits, such as tree lines, are slightly changed
286 during our simulations with increased heat flux and a warmer, open Arctic Ocean.
287 Evergreen forests around the Lake E region extend poleward to the coast and slightly
288 eastward.

289

290 **3.2.4 MIS-31 (1072 ka)**

291

292 A warm orbit with high obliquity, high eccentricity and precession aligning
293 perihelion with boreal summer allows insolation anomalies to be > 50 Wm⁻² at the
294 surface and + 60 – 80 W m⁻² (Fig. 4D) at the top of the atmosphere at the latitude of Lake
295 E. Average summer (JJA) temperatures around the lake are about +3.8 °C warmer than
296 preindustrial (Fig. 3D; Table 2). While MIS-31 is beyond the temporal range of ice core
297 greenhouse gas records, proxy geochemical records imply MIS-31 has the highest *p*CO₂
298 (~325 ppmv) of the mid-Pleistocene (Hönisch et al., 2009), contributing ~+0.80 Wm⁻²
299 relative to preindustrial values. As a result, modeled July temperatures at Lake E are >5
300 °C warmer than preindustrial temperatures.

301 Simulated precipitation at Lake E during MIS-31 is ~438 mm year⁻¹ (Table 2),
302 similar to that in MIS-11c simulations. Vegetation distribution is similar to the other
303 interglacials described here (Fig. 2E). The Lake E region is dominated by evergreen
304 taiga.

305

306 **4. Discussion**

307

308 The warm periods of Marine Isotope Stage(s) 1, 5e, 11c and 31 show similar
309 changes around Lake E. Temperature reconstructions during the Holocene Thermal
310 Maximum (9 ka) indicate +1.6 (± 0.8) °C warming in the western Arctic (Kaufman and
311 Brigham-Grette, 1993) with an overall warming of 1.7 (± 0.8) °C in the circum-Arctic
312 (Miller et al., 2010a), relative to modern temperatures. Though our model does not fully
313 account for all the warming during this period, it does produce the warming in the
314 western Arctic as documented by Kaufman and Brigham-Grette (1993). With the
315 decrease in Arctic moisture and low CO₂, deciduous and evergreen forests dominate the
316 Arctic in the model, matching the dominant vegetation such as *Alnus*, *Betula* (nut bearing
317 trees and fruits), *Poaceae* (grasses) and some birch and alder seen in the Lake E record
318 (Melles et al., 2012).

319 Marine Isotope Stage 5e produced the greatest summer warming among the four
320 interglacials simulated here. Comparisons with a preindustrial control run show that
321 differences in MTWM at Lake E during MIS-1 and 5e (+2.1 and +4.2 °C) are similar to
322 the changes seen in MIS11NG and MIS-31(+2.2 and +3.5 °C) (Table 2). Similar
323 warming has been seen in other modeling studies showing that a high obliquity and high
324 eccentricity with precession aligning perihelion with boreal summer will yield the
325 warmest boreal summer temperatures (Koenig et al., 2011; Lunt et al., 2013; Otto-
326 Bliesner et al., 2006; Yin and Berger, 2011). Strong insolation forcing at these latitudes
327 cause July maximum temperatures to exceed preindustrial temperatures by >2 °C. The 2–
328 4 °C simulated MIS-5e warming in Siberia and Lake E has also been seen in proxy data
329 compilations (CAPE, 2006; Lozhkin and Anderson (1995); Lozhkin et al. (2006)) and in
330 simulations using a GCM without vegetation feedbacks (Otto-Bliesner et al., 2006). Most
331 of the warming has been linked to the summer insolation anomaly associated with the
332 MIS-5e orbit (Otto-Bliesner et al., 2006). The exceptional summer warmth of MIS-5e
333 compared to other interglacials was previously thought to have caused a substantial
334 reduction in the GIS, however, more recent work suggests the GIS contributed only ~1.4
335 to 4.3 m of equivalent eustatic sea level rise during the LIG (Colville et al., 2011;
336 Quiquet et al., 2013; Robinson et al., 2011; Stocker et al., 2013; Stone et al., 2013), and
337 remained mostly intact (Dahl-Jensen and NEEM community members, 2013). This

338 suggests that our simulations of MIS-5e with a modern GIS are a good approximation for
339 this period. Colder and fresher sea surface conditions in the North Atlantic, Labrador and
340 Norwegian Seas have been found in marine sediments records possibly indicating
341 freshwater input (perhaps from parts of Greenland) which may have led to early LIG
342 warming attributed to stronger ocean overturning (Govin et al., 2012). In the model,
343 Arctic warming during MIS-5e allows almost a full replacement of shrub tundra with
344 deciduous forest in and around the Lake E region. Pollen analysis during this period
345 shows tree species of birch, alder, pine and spruce (Melles et al., 2012). However,
346 multiproxy studies of MIS-5e show a change in MTWM of only +2 °C compared to
347 modern temperatures (Melles et al., 2012) (Table 2). It can be concluded that the warm
348 boreal summer orbit at MIS-5e can account for much of the warmth in Beringia, and the
349 circum-Arctic, but the particularly muted response in the Lake E proxy record to summer
350 insolation forcing cannot be fully explained.

351 Simulations of MIS-11c exhibit another very warm interglacial at Lake E, with
352 MTWM maxima approaching +2.2 °C warmer than preindustrial temperatures (Table 2).
353 Similarly to MIS-5e and 1, peak warmth coincides with perihelion during boreal summer,
354 however low eccentricity and obliquity attenuates the effects of precession relative to 5e
355 and 1, making summer insolation less intense. A combination of eccentricity, obliquity
356 and precession elevates summer insolation for ~45k years, a much longer (but less
357 intense) interval of elevated summer insolation than during the other interglacials studied
358 here. The overall warmth of MIS-11 is, in part, an outcome of reduced snow and ice
359 cover.

360 Another possible mechanism contributing to Lake E warmth at MIS-11 might be
361 related to elevated sea level at this time (Raymo and Mitrovica, 2012), possibly
362 contributing to increased Bering Strait through flow. Today, the Bering Strait is limited to
363 ~50 m in depth with a net northward transport of ~0.8 Sv (Woodgate et al., 2010).
364 Oceanic heat transport into the Arctic basin might have been elevated during high sea
365 level, providing a source of warm water intrusion into the Arctic Ocean basin from the
366 North Pacific. As a simple test of the potential for a warmer Arctic Ocean with less sea
367 ice to affect temperatures over terrestrial Beringia, heat flux convergence under sea ice in
368 the Arctic Ocean was increased from 2 to 10 W m⁻². Summer sea ice fraction was

369 reduced by 25 – 50 % and summer ocean temperatures warmed by 0.2 – 1.0 °C (Fig.
370 5A,B). The simulated warming of the Arctic Ocean warmed the Lake E region, but only
371 slightly (+0.7 °C), and does not account for the exceptional warmth observed during
372 MIS-11c relative to MIS-5e.

373 The influence of MIS-11c temperatures on terrestrial biome distributions is
374 supported in model simulations by a poleward advance of evergreen needle-leaf forest
375 around the lake, which is in good agreement with palynological analysis (Melles et al.,
376 2012) showing forest-tundra and northern larch-taiga dominated by spruce, pine, birch,
377 alder and larch (Melles et al., 2012). Surface warming as a result of albedo feedbacks
378 associated with needle-leaf forests during snow-covered months accounts for some of the
379 warming during this period, however increased evergreen, terrestrial forest and enhanced
380 evapotranspiration provides a slight net cooling during the summers.

381 A deglaciated Greenland has been shown to have regional effects on SSTs and
382 sea-ice conditions, however warming of the circum-Arctic has been shown to be minimal
383 (Koenig et al., 2012; Otto-Bliesner et al., 2006). This is also demonstrated in our
384 simulations, whereby the loss of the GIS warms summer annual temperatures around
385 Lake E by only 0.3 °C (Table 2). An analysis of 500 hPa geopotential height anomalies
386 show ridging (positive height anomalies of > 10 m) to the east and troughing (negative
387 height anomalies) to the west of Lake E, indicating a slight change in the large-scale
388 planetary wave patterns over Beringia. Over Lake E, positive height anomalies are also
389 present, indicating slightly warmer conditions and a slight eastward shift of an
390 atmospheric ridge that may have been set up further west of Lake E. The ridging in these
391 simulations may also be related to a decrease in precipitation at Lake E when the GIS is
392 removed in GCM. Extended high pressure over Beringia associated with ridging would
393 create somewhat drier conditions for the region. If the exceptional warmth of MIS-11c is
394 indeed related to the melting of the GIS, freshwater input may have been a mechanism to
395 strengthen North Atlantic overturning creating the warmth missing in our simulations
396 (Govin et al., 2012). Furthermore, it is not clear why the GIS would have survived MIS-
397 5e warmth, and not MIS-11c. In sum, the exceptional Arctic warmth of MIS-11c remains
398 difficult to explain and is not a straightforward result of greenhouse gases, orbital forcing,
399 vegetation feedbacks, or Arctic Ocean warming.

400 Elevated GHG concentrations and a very warm summer orbit can explain much of
401 the warmth during MIS-31, assuming atmospheric CO₂ was higher than MIS-5e and
402 MIS-11 (Hönisch et al., 2009). In the model, the combination of elevated greenhouse
403 gases and strong summer insolation forcing at 1072 ka allow dense needle-leaf and
404 deciduous forests to grow around the Lake. Simulated summer temperatures are about 12
405 °C (Table 2), +2 °C warmer than modern summer temperatures around Lake E. Biome
406 reconstructions derived from pollen analysis of the Lake E core (Melles et al., 2012)
407 show a maxima of trees and shrubs during peak northern hemisphere insolation of MIS-
408 31 at 1072 ka. Our model simulations show similar results around Lake E, with increased
409 boreal forest and less tundra and small dwarf shrubs. The snow-albedo effect combined
410 with low-albedo forest cover allows temperatures to increase in the Arctic during MIS-
411 31. Peak precipitation rates derived from proxy analysis indicate about 600 mm year⁻¹, or
412 about 162 mm year⁻¹ more precipitation than in our preindustrial model simulation
413 (Melles et al., 2012). GCM results at MIS-31 indicate annual precipitation of ~490 mm
414 year⁻¹ (Table 2), the most annual precipitation among the four interglacials simulated
415 here. While the GCM does not fully capture the enhanced precipitation indicated in the
416 proxy record, a relative increase in precipitation is evident. Extraordinary warmth during
417 MIS-31 correlates well with a diminished WAIS (Pollard and DeConto, 2009) implying
418 strong inter-hemispheric coupling that has been related to possible reductions in Antarctic
419 Bottom Water (AABW) formation during times of ice-shelf retreat and increased fresh
420 water input into the Southern Ocean (Foldvik, 2004). WAIS collapse could also be linked
421 with the Beringian and Lake E warmth during MIS-11c and MIS-5e, but definitive
422 evidence of WAIS retreat during these later Pleistocene interglacials is currently lacking
423 (McKay et al., 2012).

424

425 **5. Conclusions**

426

427 Lake E provides a high-resolution terrestrial proxy record of climate variability in
428 the Arctic. A linked climate modeling study described here shows that Arctic summers
429 were significantly warmer during several Pleistocene interglacials by as much as + 2 °C
430 during MIS-1 and 11c, and by as much as + 4 °C during MIS-5e and 31 relative to

431 preindustrial. It can be inferred that most of the warming in the interglacial simulations
432 can be attributed to a combination of elevated GHGs and astronomical forcing, although,
433 astronomical forcing (at times producing high-intensity summer insolation $>50 \text{ Wm}^{-2}$
434 higher than today) was the dominant warming mechanism. Greenhouse gas levels during
435 MIS-31 remain poorly known, and the extreme warmth of this particular interglacial
436 could have been substantially augmented by GHG forcing. MIS-1 had relatively low CO_2
437 around the time of peak Holocene warmth, producing 0.44 Wm^{-2} less radiative forcing
438 relative to preindustrial levels (Melles et al., 2012), but the combination of orbital forcing
439 and perhaps other factors such as changes in Antarctic Bottom Water (AABW)
440 production and reduced Arctic sea-ice may have contributed to exceptional Arctic
441 warmth at this time. Thorough testing of these ideas will require additional simulations
442 with coupled atmosphere-ocean models, changes in circum-arctic ice sheets, eustatic sea-
443 levels, continentality, changes in sea-ice distributions and the addition of melt-water
444 inputs into northern and southern hemisphere oceans.

445 Extreme interglacial warmth shifted Lake E vegetation from mostly tundra with
446 small shrubs as we see the Arctic today to thick, lush evergreen and boreal forest. Due to
447 the extreme warmth, wetter conditions prevailed during the super-interglacials, allowing
448 forest biomes to thrive and increase their maximum extent poleward. While simulated
449 warming at Lake E is broadly similar during each interglacial, the vegetation response in
450 each simulation is unique, reflecting differences in seasonal temperatures and
451 hydroclimate. The simulated absence of a Greenland Ice Sheet allowed summer
452 temperatures to increase to almost $16 \text{ }^\circ\text{C}$ warmer than present over Greenland, but with
453 limited impact on temperatures around Lake E. The observed response of Beringia's
454 climate and terrestrial vegetation to super-interglacial forcing is still not fully understood
455 and creates a challenge for climate modeling and for quantifying the strength of Arctic
456 amplification. Among the interglacials studied here, MIS-11c is the warmest interglacial
457 in the Lake E record, yet MIS-5e is the warmest simulated by the model. The model
458 produces overall drier conditions in the earlier interglacials (11c and 31) than suggested
459 by pollen analysis. If the proxy interpretations were correct, this would suggest that the
460 model is missing some important regional processes. The timing of significant warming
461 in the circum-Arctic can be linked to major deglaciation events in Antarctica,

462 demonstrating possible inter-hemispheric linkages between the Arctic and Antarctic
463 climate on glacial-interglacial timescales, which have yet to be explained.

464

465

466 **References**

467

468 Alder, J. R., Hostetler, S. W., Pollard, D. and Schmittner, A.: Evaluation of a present-day
469 climate simulation with a new coupled atmosphere-ocean model GENMOM, *Geosci.*
470 *Model Dev.*, 4(1), 69–83, doi:10.5194/gmd-4-69-2011, 2011.

471 Bakker, P., Stone, E. J., Charbit, S., Gröger, M., Krebs-Kanzow, U., Ritz, S. P., Varma,
472 V., Khon, V., Lunt, D. J., Mikolajewicz, U., Prange, M., Renssen, H., Schneider, B. and
473 Schulz, M.: Last interglacial temperature evolution - a model inter-comparison, *Clim.*
474 *Past*, 9(2), 605–619, doi:10.5194/cp-9-605-2013, 2013.

475 Berger, A.: Long-Term Variations of Daily Insolation and Quaternary Climatic Changes,
476 *J. Atmospheric Sci.*, 35(12), 2362–2367, doi:10.1175/1520-
477 0469(1978)035<2362:LTVODI>2.0.CO;2, 1978.

478 Brigham-Grette, J., Melles, M., Minyuk, P., Andreev, A., Tarasov, P., DeConto, R.,
479 Koenig, S., Nowaczyk, N., Wennrich, V., Rosen, P., Haltia, E., Cook, T., Gebhardt, C.,
480 Meyer-Jacob, C., Snyder, J. and Herzschuh, U.: Pliocene Warmth, Polar Amplification,
481 and Stepped Pleistocene Cooling Recorded in NE Arctic Russia, *Science*, 340(6139),
482 1421–1427, doi:10.1126/science.1233137, 2013.

483 Colville, E. J., Carlson, A. E., Beard, B. L., Hatfield, R. G., Stoner, J. S., Reyes, A. V.
484 and Ullman, D. J.: Sr-Nd-Pb Isotope Evidence for Ice-Sheet Presence on Southern
485 Greenland During the Last Interglacial, *Science*, 333(6042), 620–623,
486 doi:10.1126/science.1204673, 2011.

487 Cronin, T. M., Polyak, L., Reed, D., Kandiano, E. S., Marzen, R. E. and Council, E. A.:
488 A 600-ka Arctic sea-ice record from Mendeleev Ridge based on ostracodes, *Sea Ice*
489 *Paleoclimate Syst. Chall. Reconstr. Sea Ice Proxies*, 79(0), 157–167,
490 doi:10.1016/j.quascirev.2012.12.010, 2013.

491 Dahl-Jensen, D. and NEEM community members: Eemian interglacial reconstructed
492 from a Greenland folded ice core, *Nature*, 493(7433), 489–494, doi:10.1038/nature11789,
493 2013.

494 DeConto, R. M., Galeotti, S., Pagani, M., Tracy, D., Schaefer, K., Zhang, T., Pollard, D.
495 and Beerling, D. J.: Past extreme warming events linked to massive carbon release from
496 thawing permafrost, *Nature*, 484(7392), 87–91, doi:10.1038/nature10929, 2012.

- 497 Elias, S. A. and Matthews Jr., J. V.: Arctic North American seasonal temperatures from
498 the latest Miocene to the Early Pleistocene, based on mutual climatic range analysis of
499 fossil beetle assemblages, *Can. J. Earth Sci.*, 39(6), 911–920, doi:10.1139/e01-096, 2002.
- 500 Foldvik, A.: Ice shelf water overflow and bottom water formation in the southern
501 Weddell Sea, *J. Geophys. Res.*, 109(C2), doi:10.1029/2003JC002008, 2004.
- 502 Govin, A., Braconnot, P., Capron, E., Cortijo, E., Duplessy, J.-C., Jansen, E., Labeyrie,
503 L., Landais, A., Marti, O., Michel, E., Mosquet, E., Risebrobakken, B., Swingedouw, D.
504 and Waelbroeck, C.: Persistent influence of ice sheet melting on high northern latitude
505 climate during the early Last Interglacial, *Clim. Past*, 8(2), 483–507, doi:10.5194/cp-8-
506 483-2012, 2012.
- 507 Groll, N., Widmann, M., Jones, J. M., Kaspar, F. and Lorenz, S. J.: Simulated
508 relationships between regional temperatures and large-scale circulation: 125 kyr BP
509 (Eemian) and the preindustrial period, *J. Clim.*, 18(19), 4032–4045, 2005.
- 510 Hönlisch, B., Hemming, N. G., Archer, D., Siddall, M. and McManus, J. F.: Atmospheric
511 Carbon Dioxide Concentration Across the Mid-Pleistocene Transition, *Science*,
512 324(5934), 1551–1554, doi:10.1126/science.1171477, 2009.
- 513 Howard, W. R.: Palaeoclimatology: A warm future in the past, *Nature*, 388(6641), 418–
514 419, 1997.
- 515 Kaplan, J. O.: Climate change and Arctic ecosystems: 2. Modeling, paleodata-model
516 comparisons, and future projections, *J. Geophys. Res.*, 108(D19),
517 doi:10.1029/2002JD002559, 2003.
- 518 Kaufman, D. S. and Brigham-Grette, J.: Aminostratigraphic correlations and
519 paleotemperature implications, Pliocene-Pleistocene high-sea-level deposits,
520 northwestern Alaska, *Quat. Sci. Rev.*, 12(1), 21–33, doi:10.1016/0277-3791(93)90046-O,
521 1993.
- 522 Kitoh, A. and Murakami, S.: Tropical Pacific climate at the mid-Holocene and the Last
523 Glacial Maximum simulated by a coupled ocean-atmosphere general circulation model,
524 *Paleoceanography*, 17(3), 19–1–19–13, doi:10.1029/2001PA000724, 2002.
- 525 Koenig, S. J., DeConto, R. M. and Pollard, D.: Late Pliocene to Pleistocene sensitivity of
526 the Greenland Ice Sheet in response to external forcing and internal feedbacks, *Clim.
527 Dyn.*, 37(5-6), 1247–1268, doi:10.1007/s00382-011-1050-0, 2011.
- 528 Koenig, S. J., DeConto, R. M. and Pollard, D.: Pliocene Model Intercomparison Project
529 Experiment 1: implementation strategy and mid-Pliocene global climatology using
530 GENESIS v3.0 GCM, *Geosci. Model Dev.*, 5(1), 73–85, doi:10.5194/gmd-5-73-2012,
531 2012.
- 532 Kolosova, L.: Geographical Atlas, 1980.

- 533 Langebroek, P. M. and Nisancioglu, K. H.: Simulating last interglacial climate with
534 NorESM: role of insolation and greenhouse gases in the timing of peak warmth, *Clim.*
535 *Past*, 10(4), 1305–1318, doi:10.5194/cp-10-1305-2014, 2014.
- 536 Lisiecki, L. E. and Raymo, M. E.: A Pliocene-Pleistocene stack of 57 globally distributed
537 benthic $\delta^{18}\text{O}$ records, *Paleoceanography*, 20(1), PA1003, doi:10.1029/2004PA001071,
538 2005.
- 539 Louergue, L., Schilt, A., Spahni, R., Masson-Delmotte, V., Blunier, T., Lemieux, B.,
540 Barnola, J.-M., Raynaud, D., Stocker, T. F. and Chappellaz, J.: Orbital and millennial-
541 scale features of atmospheric CH_4 over the past 800,000 years, *Nature*, 453(7193), 383–
542 386, doi:10.1038/nature06950, 2008.
- 543 Lozhkin, A. V. and Anderson, P. M.: The Last Interglaciation in Northeast Siberia,
544 *Quaternary Research*, 43, 147–158, 1995.
- 545 Lozhkin, A. V., Anderson, P. M., Matrosova, T. V. and Minyuk, P. S.: The pollen record
546 from El'gygytyn Lake: implications for vegetation and climate histories of northern
547 Chukotka since the late middle Pleistocene, *J. Paleolimnol.*, 37(1), 135–153,
548 doi:10.1007/s10933-006-9018-5, 2006.
- 549 Lunt, D. J., Abe-Ouchi, A., Bakker, P., Berger, A., Braconnot, P., Charbit, S., Fischer, N.,
550 Herold, N., Jungclaus, J. H., Khon, V. C., Krebs-Kanzow, U., Langebroek, P. M.,
551 Lohmann, G., Nisancioglu, K. H., Otto-Bliesner, B. L., Park, W., Pfeiffer, M., Phipps, S.
552 J., Prange, M., Rachmayani, R., Renssen, H., Rosenbloom, N., Schneider, B., Stone, E. J.,
553 Takahashi, K., Wei, W., Yin, Q. and Zhang, Z. S.: A multi-model assessment of last
554 interglacial temperatures, *Clim Past*, 9(2), 699–717, doi:10.5194/cp-9-699-2013, 2013.
- 555 Lüthi, D., Le Floch, M., Bereiter, B., Blunier, T., Barnola, J.-M., Siegenthaler, U.,
556 Raynaud, D., Jouzel, J., Fischer, H., Kawamura, K. and Stocker, T. F.: High-resolution
557 carbon dioxide concentration record 650,000–800,000 years before present, *Nature*,
558 453(7193), 379–382, doi:10.1038/nature06949, 2008.
- 559 McKay, R., Naish, T., Powell, R., Barrett, P., Scherer, R., Talarico, F., Kyle, P., Monien,
560 D., Kuhn, G., Jackolski, C. and Williams, T.: Pleistocene variability of Antarctic Ice
561 Sheet extent in the Ross Embayment, *Quat. Sci. Rev.*, 34, 93–112,
562 doi:10.1016/j.quascirev.2011.12.012, 2012.
- 563 Melles, M., Brigham-Grette, J., Minyuk, P. S., Nowaczyk, N. R., Wennrich, V.,
564 DeConto, R. M., Anderson, P. M., Andreev, A. A., Coletti, A., Cook, T. L., Haltia-Hovi,
565 E., Kukkonen, M., Lozhkin, A. V., Rosen, P., Tarasov, P., Vogel, H. and Wagner, B.: 2.8
566 Million Years of Arctic Climate Change from Lake El'gygytyn, NE Russia, *Science*,
567 337(6092), 315–320, doi:10.1126/science.1222135, 2012.
- 568 Miller, G. H., Alley, R. B., Brigham-Grette, J., Fitzpatrick, J. J., Polyak, L., Serreze, M.
569 C. and White, J. W. C.: Arctic amplification: can the past constrain the future?, *Quat. Sci.*
570 *Rev.*, 29(15-16), 1779–1790, doi:10.1016/j.quascirev.2010.02.008, 2010a.

571 Miller, G. H., Brigham-Grette, J., Alley, R. B., Anderson, L., Bauch, H. A., Douglas, M.
572 S. V., Edwards, M. E., Elias, S. A., Finney, B. P., Fitzpatrick, J. J., Funder, S. V.,
573 Herbert, T. D., Hinzman, L. D., Kaufman, D. S., MacDonald, G. M., Polyak, L., Robock,
574 A., Serreze, M. C., Smol, J. P., Spielhagen, R., White, J. W. C., Wolfe, A. P. and Wolff,
575 E. W.: Temperature and precipitation history of the Arctic, *Spec. Theme Arct.*
576 *Palaeoclim. Synth.* PP 1674-1790, 29(15–16), 1679–1715,
577 doi:10.1016/j.quascirev.2010.03.001, 2010b.

578 Nolan, M. and Brigham-Grette, J.: Basic hydrology, limnology, and meteorology of
579 modern Lake El'gygytgyn, Siberia, *J. Paleolimnol.*, 37(1), 17–35, doi:10.1007/s10933-
580 006-9020-y, 2006.

581 Otto-Bliesner, B. L., Marshall, S. J., Overpeck, J. T., Miller, G. H., Hu, A. and CAPE
582 Last Interglacial Project Members: Simulating Arctic Climate Warmth and Icefield
583 Retreat in the Last Interglaciation, *Science*, 311(5768), 1751–1753,
584 doi:10.1126/science.1120808, 2006.

585 Pollard, D. and DeConto, R. M.: Modelling West Antarctic ice sheet growth and collapse
586 through the past five million years, *Nature*, 458(7236), 329–332,
587 doi:10.1038/nature07809, 2009.

588 Polyak, L., Alley, R. B., Andrews, J. T., Brigham-Grette, J., Cronin, T. M., Darby, D. A.,
589 Dyke, A. S., Fitzpatrick, J. J., Funder, S., Holland, M., Jennings, A. E., Miller, G. H.,
590 O'Regan, M., Saville, J., Serreze, M., St. John, K., White, J. W. C. and Wolff, E.:
591 History of sea ice in the Arctic, *Spec. Theme Arct. Palaeoclim. Synth.* PP 1674-1790,
592 29(15–16), 1757–1778, doi:10.1016/j.quascirev.2010.02.010, 2010.

593 Prokopenko, A. A., Bezrukova, E. V., Khursevich, G. K., Solotchina, E. P., Kuzmin, M.
594 I. and Tarasov, P. E.: Climate in Continental Interior Asia During the Longest Interglacial
595 of the Past 500000 Years: The New MIS 11 Records from Lake Baikal, SE Siberia, *Clim*
596 *Past*, 6, 31–48, 2010.

597 Quiquet, A., Ritz, C., Punge, H. J. and Salas y Méliá, D.: Greenland ice sheet
598 contribution to sea level rise during the last interglacial period: a modelling study driven
599 and constrained by ice core data, *Clim Past*, 9(1), 353–366, doi:10.5194/cp-9-353-2013,
600 2013.

601 Raymo, M. E. and Mitrovica, J. X.: Collapse of polar ice sheets during the stage 11
602 interglacial, *Nature*, 483(7390), 453–456, doi:10.1038/nature10891, 2012.

603 Robinson, A., Calov, R. and Ganopolski, A.: Greenland ice sheet model parameters
604 constrained using simulations of the Eemian Interglacial, *Clim Past*, 7(2), 381–396,
605 doi:10.5194/cp-7-381-2011, 2011.

606 Scherer, R. P., Bohaty, S. M., Dunbar, R. B., Esper, O., Flores, J.-A., Gersonde, R.,
607 Harwood, D. M., Roberts, A. P. and Taviani, M.: Antarctic records of precession-paced
608 insolation-driven warming during early Pleistocene Marine Isotope Stage 31, *Geophys.*
609 *Res. Lett.*, 35(3), doi:10.1029/2007GL032254, 2008.

610 Schilt, A., Baumgartner, M., Blunier, T., Schwander, J., Spahni, R., Fischer, H. and
611 Stocker, T. F.: Glacial–interglacial and millennial-scale variations in the atmospheric
612 nitrous oxide concentration during the last 800,000 years, *Quat. Sci. Rev.*, 29(1-2), 182–
613 192, doi:10.1016/j.quascirev.2009.03.011, 2010.

614 Serreze, M. C. and Hurst, C. M.: Representation of Mean Arctic Precipitation from
615 NCEP–NCAR and ERA Reanalyses, *J. Clim.*, 13(1), 182–201, doi:10.1175/1520-
616 0442(2000)013<0182:ROMAPF>2.0.CO;2, 2000.

617 Stocker, T. F., Qin, D., Plattner, G.-K., Tignor, M., Allen, S. K., Boschung, J., Nauels,
618 A., Xia, Y., Bex, V. and Midgley (eds.), P. .: IPCC,2013: Climate Change 2013: The
619 Physical Science Basis. Contribution of Working Group I to the Fifth Assessment Report
620 of the Intergovernmental Panel on Climate Change, Camb. Univ. Press Camb. UK N. Y.
621 NY USA, 1535 pp, doi:10.1017/CBO9781107415324, 2013.

622 Stone, E. J., Lunt, D. J., Annan, J. D. and Hargreaves, J. C.: Quantification of the
623 Greenland ice sheet contribution to Last Interglacial sea level rise, *Clim Past*, 9(2), 621–
624 639, doi:10.5194/cp-9-621-2013, 2013.

625 Tarasov, P. E., Nakagawa, T., Demske, D., Österle, H., Igarashi, Y., Kitagawa, J.,
626 Mokhova, L., Bazarova, V., Okuda, M., Gotanda, K., Miyoshi, N., Fujiki, T., Takemura,
627 K., Yonenobu, H. and Fleck, A.: Progress in the reconstruction of Quaternary climate
628 dynamics in the Northwest Pacific: A new modern analogue reference dataset and its
629 application to the 430-kyr pollen record from Lake Biwa, *Earth-Sci. Rev.*, 108(1-2), 64–
630 79, doi:10.1016/j.earscirev.2011.06.002, 2011.

631 Thompson, S. L. and Pollard, D.: Greenland and Antarctic mass balances for present and
632 doubled atmospheric CO₂ from the GENESIS version-2 global climate model, *J. Clim.*,
633 10(5), 871–900, 1997.

634 De Vernal, A. and Hillaire-Marcel, C.: Natural Variability of Greenland Climate,
635 Vegetation, and Ice Volume During the Past Million Years, *Science*, 320(5883), 1622–
636 1625, doi:10.1126/science.1153929, 2008.

637 Viereck, L. A. and Little Jr, E. L.: Atlas of United States Trees, Volume 2: Alaska Trees
638 and Common Shrubs., 1975.

639 Willerslev, E., Cappellini, E., Boomsma, W., Nielsen, R., Hebsgaard, M. B., Brand, T.
640 B., Hofreiter, M., Bunce, M., Poinar, H. N., Dahl-Jensen, D., Johnsen, S., Steffensen, J.
641 P., Bennike, O., Schwenninger, J.-L., Nathan, R., Armitage, S., de Hoog, C.-J., Alfimov,
642 V., Christl, M., Beer, J., Muscheler, R., Barker, J., Sharp, M., Penkman, K. E. H., Haile,
643 J., Taberlet, P., Gilbert, M. T. P., Casoli, A., Campani, E. and Collins, M. J.: Ancient
644 Biomolecules from Deep Ice Cores Reveal a Forested Southern Greenland, *Science*,
645 317(5834), 111–114, doi:10.1126/science.1141758, 2007.

646 Woodgate, R. A., Weingartner, T. and Lindsay, R.: The 2007 Bering Strait oceanic heat
647 flux and anomalous Arctic sea-ice retreat, *Geophys. Res. Lett.*, 37(1), n/a–n/a,
648 doi:10.1029/2009GL041621, 2010.

649 Yin, Q. Z. and Berger, A.: Individual contribution of insolation and CO2 to the
 650 interglacial climates of the past 800,000 years, *Clim. Dyn.*, 38(3-4), 709–724,
 651 doi:10.1007/s00382-011-1013-5, 2011.

652

653

654

655

656

657

658 **Figures:**

659

660

661

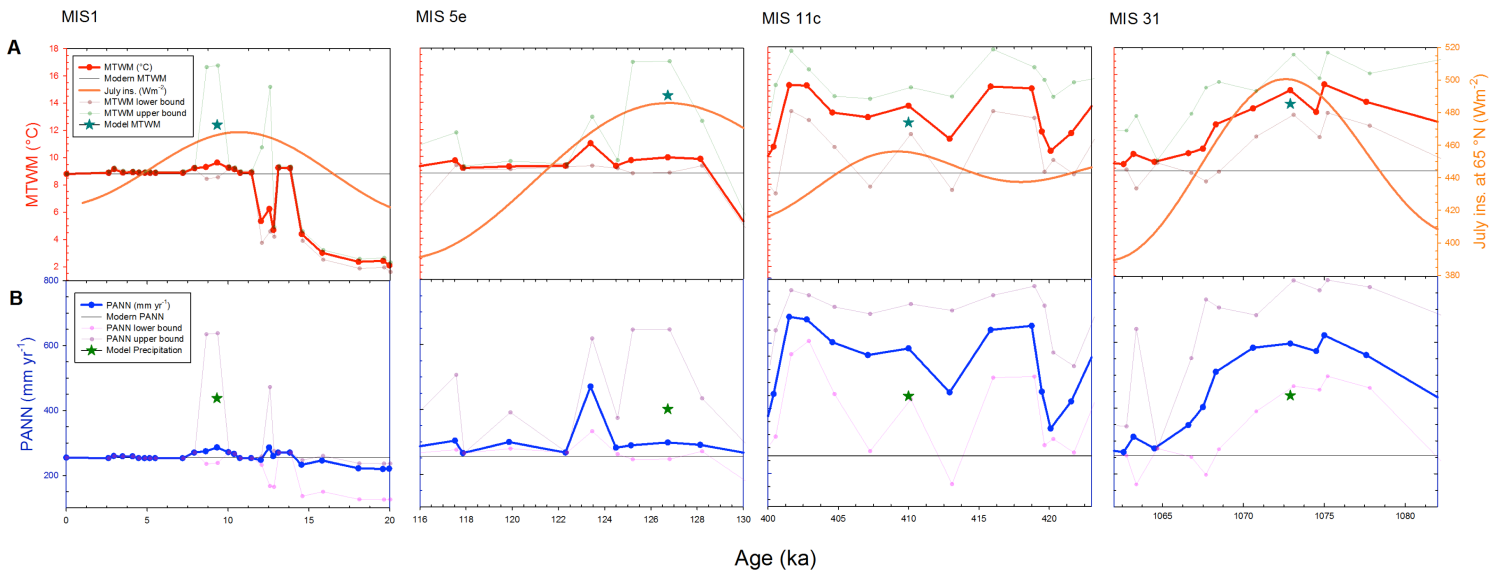


Figure 1: (A and B) A Reconstructed MTWM and B PANN from Melles et al., 2012. Transparent data above and below the bolded lines are upper and lower limits of each data point calculated from a best modern analogue technique (MAT) function. The dark cyan (A) and dark green (B) stars denote results from the GCM simulations with respect to MTWM and PANN.

662

663

664

665

666

667

668

669

670

671

672

673
674
675

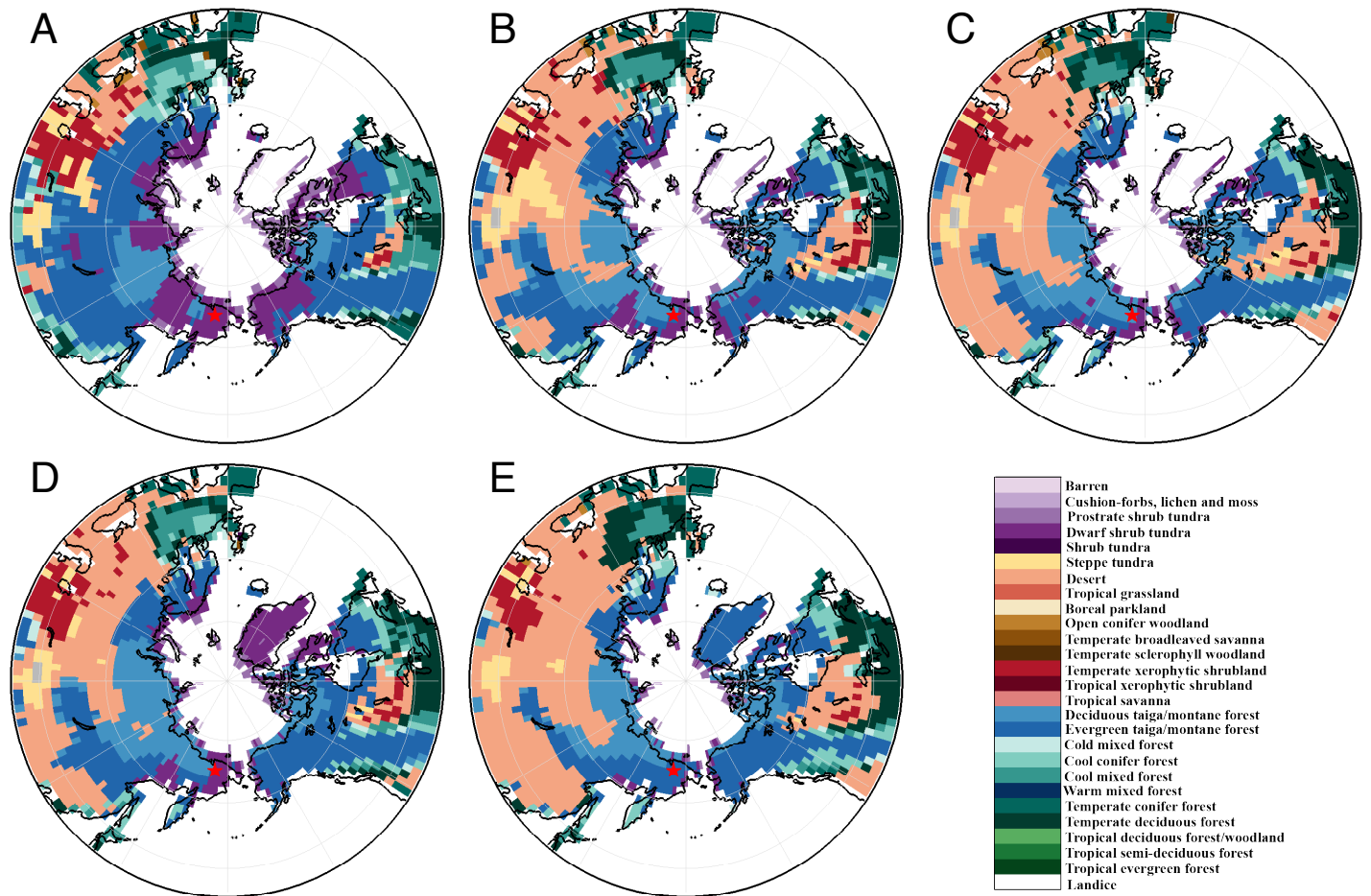
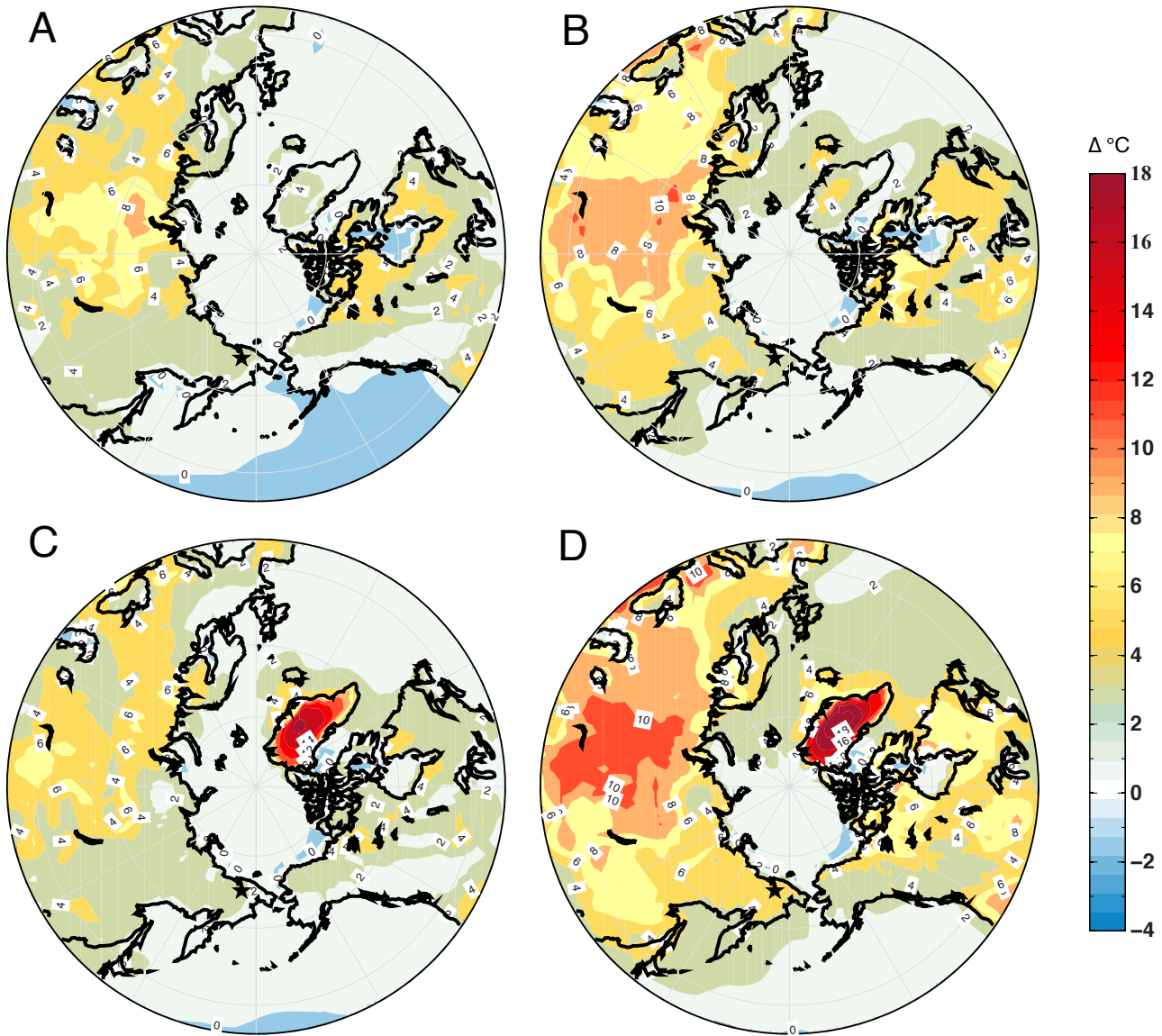


Figure 2: Distribution of interglacial vegetation simulated by the BIOME4 interactive vegetation model coupled to the GCM. A Preindustrial vegetation corresponding to a modern orbit, **B** MIS-1 (9 ka), **C** MIS-5e vegetation, **D** MIS11NG vegetation and **E** MIS-31 (no GIS) vegetation. The location of Lake E is shown near the bottom of each figure with a red star. Note the poleward advancement of evergreen and needle-leaf trees around the lake during each interglacial and the replacement of shrub tundra to taiga forest. (*vegetation data from Melles et al., 2012*).

676
677
678
679
680
681
682
683
684

685
686

687



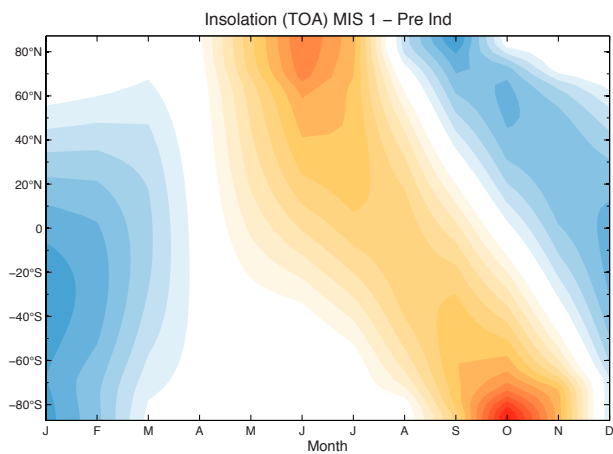
692

Figure 3: Simulated interglacial anomalies (2-meter annual air temperature in $^{\circ}\text{C}$) relative to preindustrial temperatures. A MIS-1 (9 ka orbit and GHGs), B MIS-5e (127 ka orbit and GHGs), C MIS-11c (409 ka orbit and GHGs, and no Greenland Ice Sheet), D MIS-31 (1072 ka orbit and GHGs, and no Greenland Ice Sheet). The location of Lake El'gygytyn (black star) is shown near the bottom of each panel. Areas of no shading (white) roughly correspond to no change that is statistically significant at the 95% confidence interval.

693
694
695

696
697
698
699
700
701

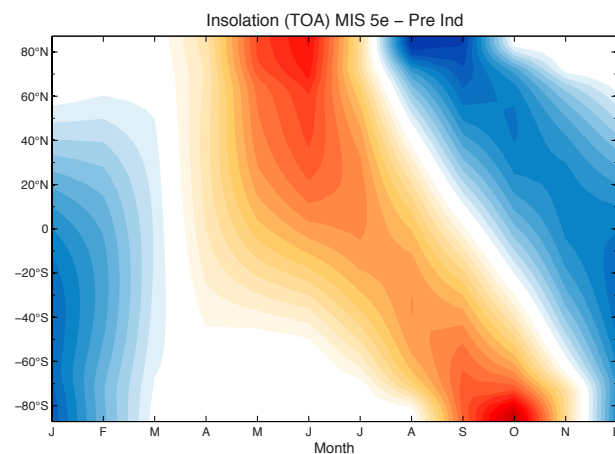
A



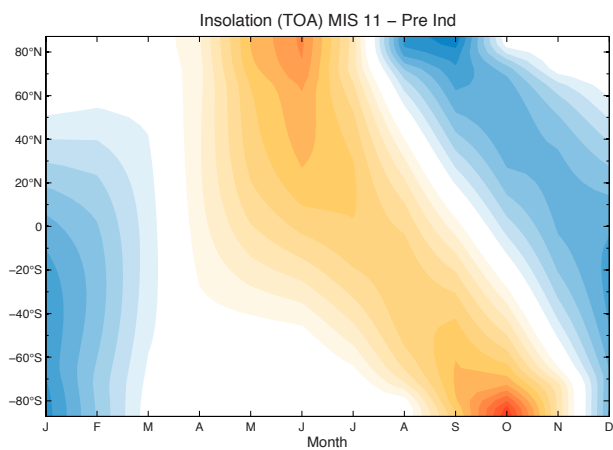
702

B

703

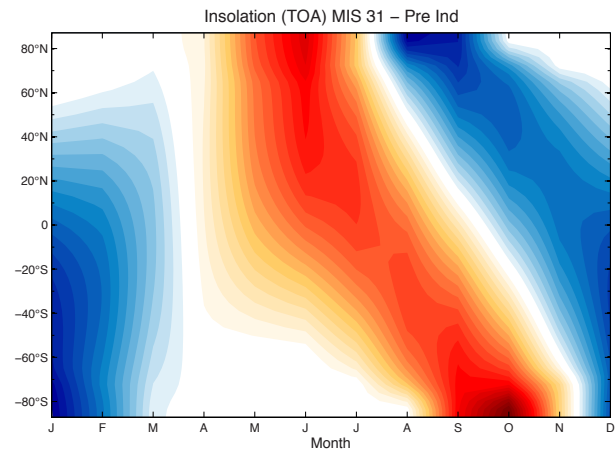


C



D

704



705
706
707

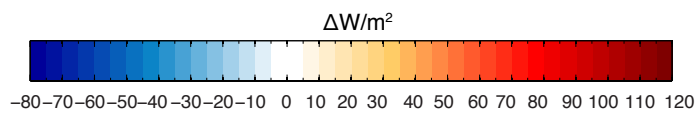


Figure 4: Monthly insolation anomalies at the top of the atmosphere for the interglacial intervals modeled here [W/m^2]. A MIS-1 anomalies with respect to preindustrial (modern) orbit, B MIS-5e anomalies with respect to preindustrial orbit, C MIS-11c anomalies with respect to preindustrial orbit and D MIS-31 anomalies with respect to preindustrial orbit.

708
709
710
711

712
713
714
715
716
717
718
719
720
721
722
723
724
725
726
727
728
729
730
731
732
733
734
735
736
737
738
739
740
741
742
743
744
745
746
747
748
749
750
751
752
753
754
755
756
757
758
759
760
761
762

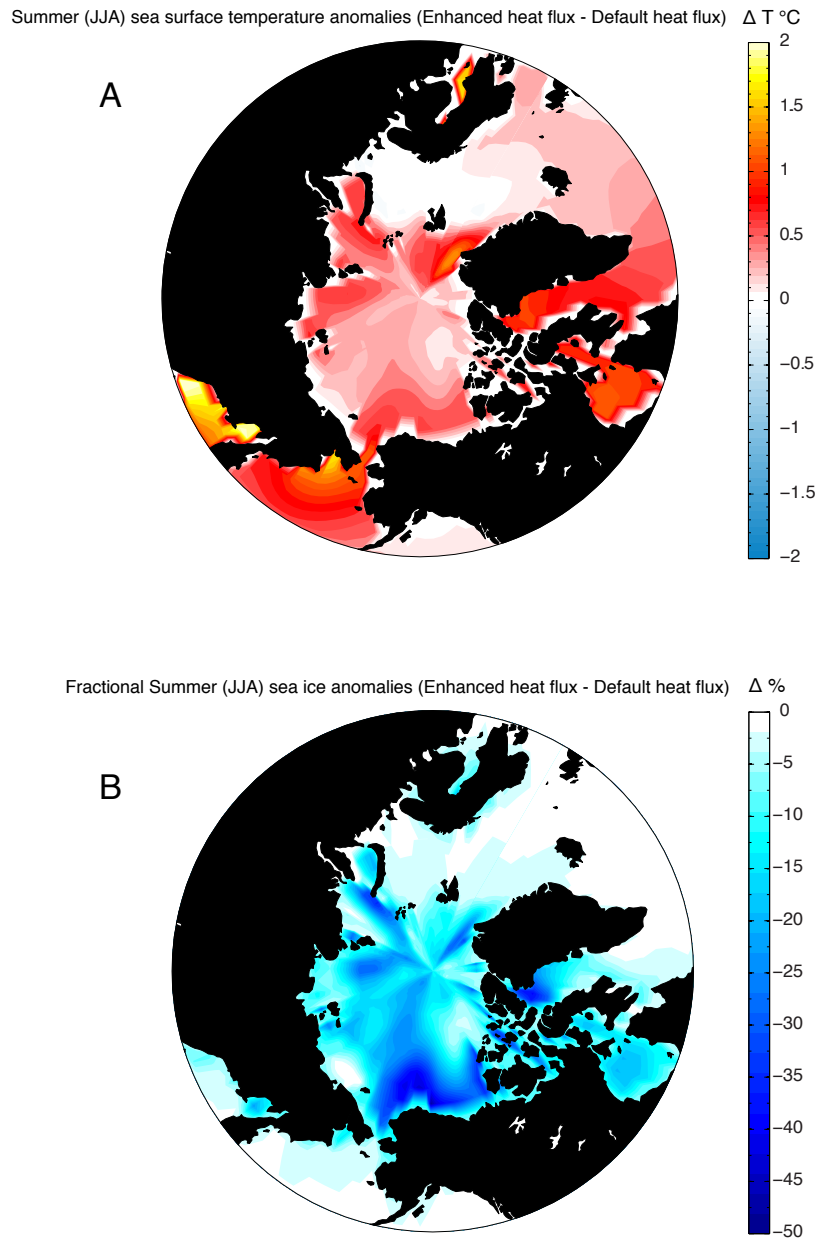


Figure 5: Model simulated (MIS11NG) Summer sea surface temperature and sea ice anomalies caused by enhanced oceanic heat flux (+8 W/m²) at 409 ka. A Summer (JJA) sea surface temperature change with respect to default heat flux simulation (T °C) and B Summer (JJA) sea ice fraction anomalies (%) with respect to default heat flux simulation. With +8 W/m² of sub-sea ice heat flux convergence, Arctic Ocean SSTs rise > 0.5 °C and sea ice fraction decreases 25-50% in most areas.

763
764
765
766
767
768

Table 1: Overview of interglacial simulations performed during this study. Orbital configurations (Bergert 1978) and greenhouse gas (GHG) concentrations (Honisch et al., 2009; Loulergue et al., 2008; Lüthi et al., 2008 Schilt et al., 2010). Modern GHG concentrations are taken from 1950 AD; obliquity is given in degrees and precession (Ω) in degrees.

Age	Run description	CO ₂ (ppmv)	CH ₄ (ppbv)	N ₂ O (ppbv)	Eccentricity	Obliquity (°)	Precession (Ω , °)
1850 AD	pre-industrial simulation with pre-industrial GHG concentrations	280	801	289	0.01671	23.438	101.37
9 ka	MIS 1 - with (modern) GIS	~260	~611	~263	0.01920	24.229	310.32
127 ka	MIS 5e - with (modern) GIS	287	724	262	0.03938	24.040	272.92
409 ka	MIS 11c - with (modern) GIS	285	713	285	0.01932	23.781	265.34
409 ka	MIS 11c - no GIS	285	713	285	0.01932	23.781	265.34
409 ka	MIS 11c - no GIS + 10 Wm ⁻² increase of heat flux under sea ice	285	713	285	0.01932	23.781	265.34
1072 ka	MIS 31 - with no GIS	325	800	288	0.05597	23.898	289.79

769
770
771
772
773
774
775
776
777
778
779
780
781
782
783
784
785
786
787
788
789
790
791
792
793
794
795
796
797

798
 799
 800
 801
 802
 803
 804

Table 2: List of GCM simulations with corresponding variables at the grid cell location of Lake E. Mean Annual Air Temperature (MAAT), Summer temperature (JJA), Mean Temperature of the Warmest Month (MTWM; July) and Mean Annual Precipitation (PANN) are listed below.

Run	Pre-industrial	MIS 1-with GIS	MIS 5e-with GIS	MIS 11c-with GIS	MIS 11c-no GIS	MIS 11c-noGIS-10Wm ⁻²	MIS 31-without GIS
Lake-E							
MAAT (°C)	-12	-12	-12.4	-11.5	-12.5	-10.5	-10.4
Summer Temp (JJA; °C)	8	9.6	10.5	10	10.2	10.5	11.8
MTWM (July, °C)	10.3	12.4	14.5	12.2	12.5	13.2	13.8
PANN (mm yr ⁻¹)	438	438	401	475	438	475	438